

A. SUPPLEMENTARY MATERIAL

A.1 Convective heat transfer coefficient and Biot number for different ranges of superficial air speed

For our conceptual study to identify the differences between various packages, we considered indicative ranges for every unit operation. A value of the superficial air speed at the inlet was set to $0.01 \text{ m}\cdot\text{s}^{-1}$ for retail and refrigerated storage, $0.1 \text{ m}\cdot\text{s}^{-1}$ for refrigerated transport, and $1.0 \text{ m}\cdot\text{s}^{-1}$ for pre-cooling (Han et al., 2017; Li et al., 2021; Opara and Zou, 2007; Thompson et al., 2008; Wu et al., 2019). The convective heat transfer coefficients and Biot numbers corresponding to these ranges of superficial air speed are presented in Figure A1. The convective heat transfer coefficients are in the same range as those estimated for strawberries in other studies (Silva et al., 2017).

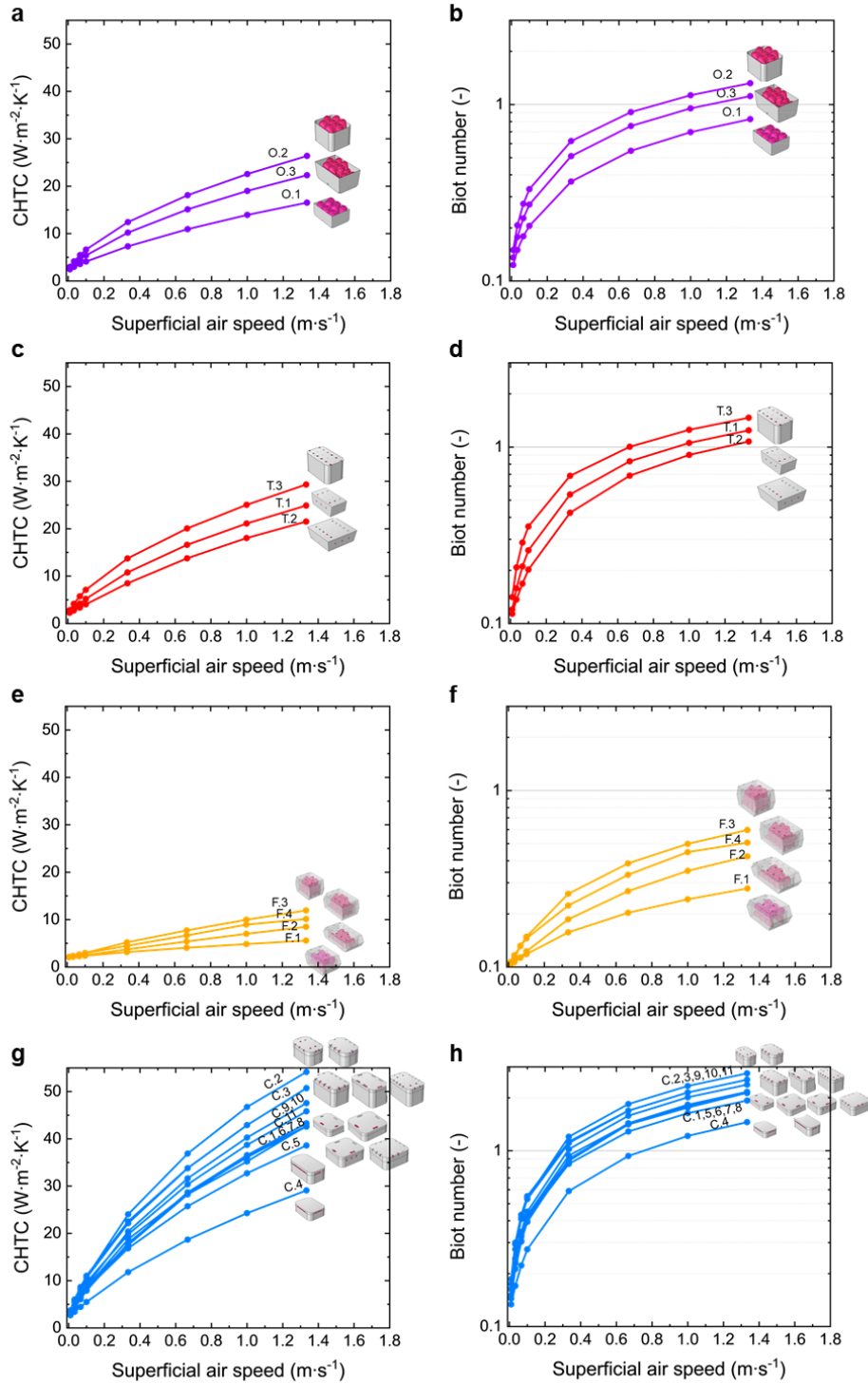


Figure A1: Plots for the convective heat transfer coefficient (CHTC, $\text{W}\cdot\text{m}^{-2}\cdot\text{K}^{-1}$) and Biot number ($=\text{CHTC}\cdot D/k_f$) as a function of superficial air speed for different packages.

A.2 Calibration of the kinetic quality model

The calibration of the respiration-driven kinetic quality model is presented in Figure A2. In brief, strawberries can be stored for about 14 days at 0 °C, for 5 days at 10 °C, and for about 2 days at 20 °C.

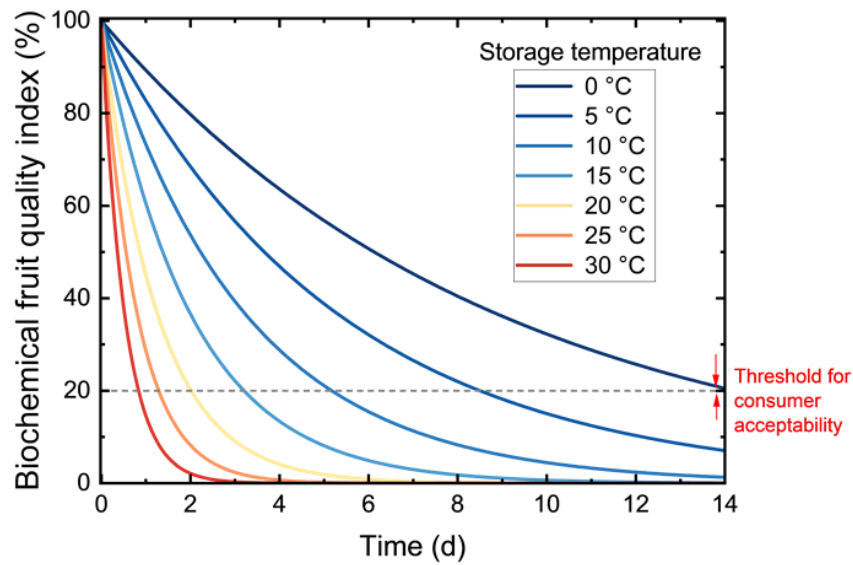


Figure A2: Temporal evolution of the overall respiration-driven fruit quality index for strawberries at different constant storage temperatures, which was used to calibrate our kinetic model. In our calibration, the threshold for consumer acceptability at which fruit reach the end of shelf life is arbitrarily set to a quality index value of 20%.

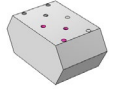
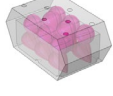
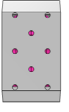
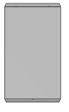


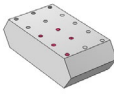
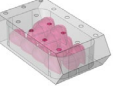




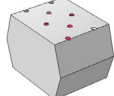

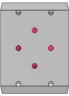



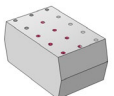
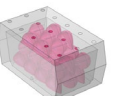










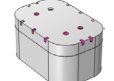

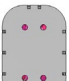
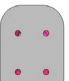


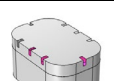





A.3 Packaging configurations

Table A1: Detailed summary of the 21 packages evaluated in this study. The packages were divided into four major types: open punnet trays (O), top-sealed recloseable trays (T), flow-wrapped packages (F), and ventilated clamshells (C).

Package name	Isometric view	Isometric translucent view	Top view	Bottom view	Side view 1	Side view 2	Intended weight of fruit (g)	Packaging material	TOA for entire package (%)	Headspace volume (%)	Length:width ratio (-)	TOA in flow direction (%)
Open punnet trays (O)												
O.1							250	Paperboard	25.14	71.94*	1.44	0.56
O.2							400	R-PET	20.88	61.39*	1.18	0
O.3							500	Paperboard	25.27	62.95*	1.60	0.28
Top-sealed trays (T)												
T.1							250	Paperboard, PP film	0.82	83.84	1.89	0.52
T.2							300	Paperboard, PP film	1.05	77.94	1.00	0.78
T.3							500	R-PET, PP film	1.09	61.99	1.68	1.09

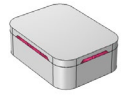



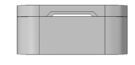
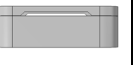

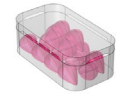







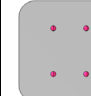



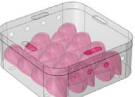

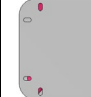

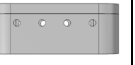
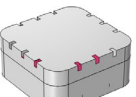
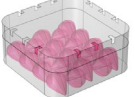

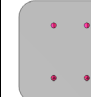


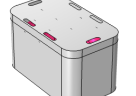
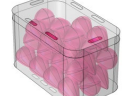
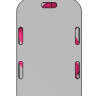
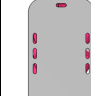

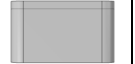
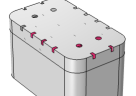
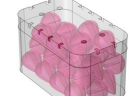
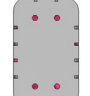



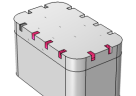
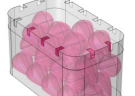
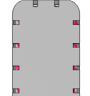


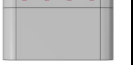
TOA, total open area; *for open trays, the volume of package was estimated by considering the height of a reusable packaging crate (IFCO, 2022) which is 10.5 cm. R-PET, recycled polyethylene terephthalate; PP, polypropylene.

Supplementary Material

Package name	Isometric view	Isometric translucent view	Top view	Bottom view	Side view 1	Side view 2	Weight of fruit (g)	Packaging material	TOA for entire package (%)	Headspace volume (%)	Length:width ratio (-)	TOA in flow direction (%)
Flow-wrapped packages (F)												
F.1							250	Paperboard, LDPE film	0.67	74.21	1.78	0.00
F.2							250	R-PET, LDPE film	1.21	74.76	2.05	0.00
F.3							400	R-PET, LDPE film	0.56	67.91	1.47	0.00
F.4							500	Paperboard, LDPE film	0.97	68.54	2.29	0.00
Ventilated clamshells (C)												
C.1							250	R-PET	1.92	63.69	1.33	0.00
C.2							250	R-PET	1.61	64.96	1.50	0.24
C.3							250	R-PET	1.44	64.96	1.50	0.54

TOA, total open area; LDPE, low-density polyethylene; R-PET, recycled polyethylene terephthalate.

Supplementary Material

Package name	Isometric view	Isometric translucent view	Top view	Bottom view	Side view 1	Side view 2	Weight of fruit (g)	Packaging material	TOA for package (%)	Headspace volume (%)	Length: width ratio (-)	TOA in flow direction (%)
(...continued) Ventilated clamshells (C)												
C.4							250	R-PET	1.84	72.07	1.33	1.06
C.5							250	R-PET	2.05	71.07	1.79	1.39
C.6							300	R-PET	1.59	63.94	1.00	0.00
C.7							300	R-PET	2.49	75.96	1.00	0.49
C.8							300	R-PET	1.68	80.24	1.00	0.36
C.9							500	R-PET	2.00	62.39	1.68	0.00
C.10							500	R-PET	0.97	61.58	1.68	0.17
C.11							500	R-PET	1.50	61.58	1.68	0.26

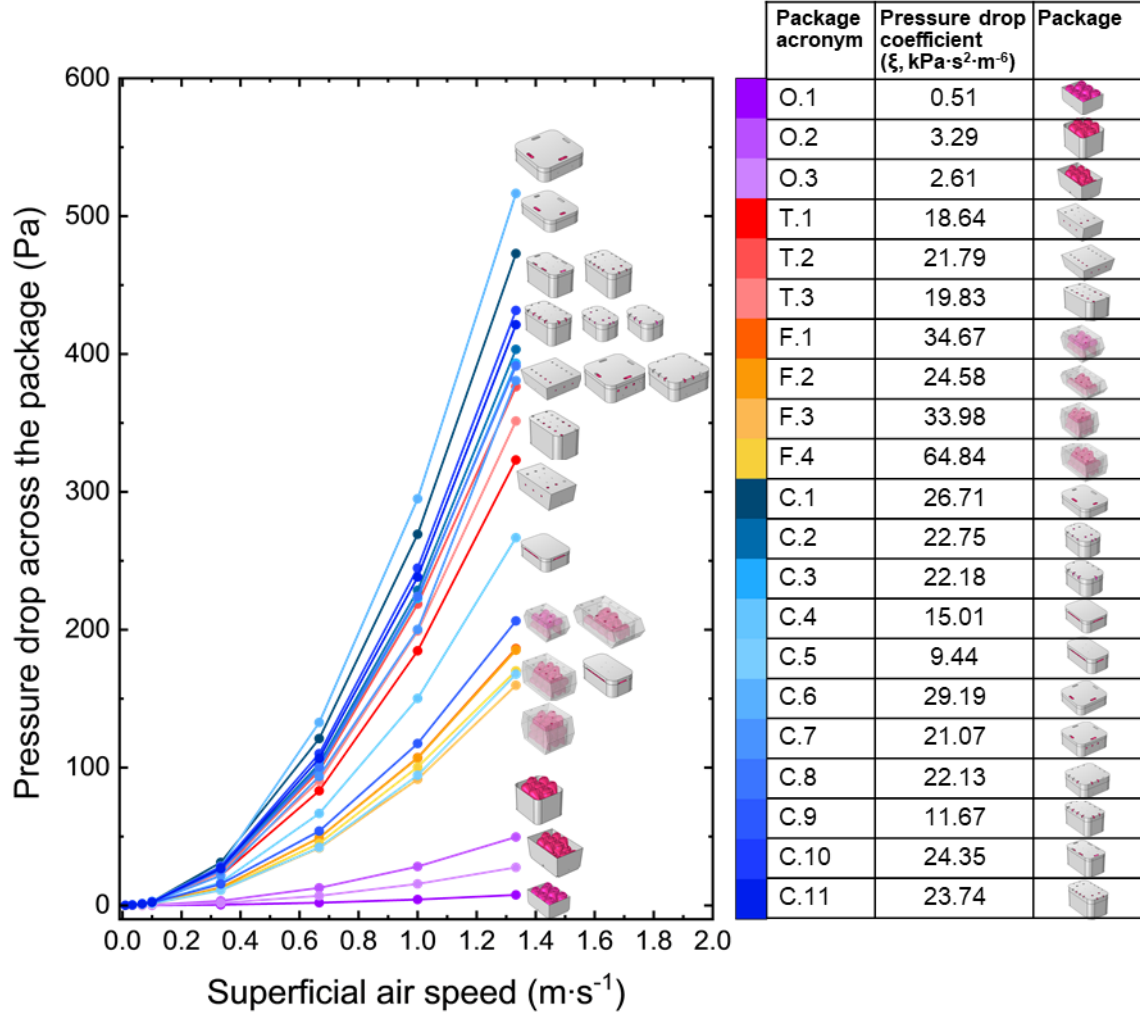
TOA, total open area; R-PET, recycled polyethylene terephthalate.

A.4 Pressure drop across the package

The pressure drop (ΔP , Pa) was evaluated at two points at a distance of 5 cm before and after the package in the channel. A parametric study was carried out for superficial air speeds of 0.01, 0.033, 0.067, 0.1, 0.33, 0.67, 1.0, and 1.33 $\text{m}\cdot\text{s}^{-1}$. The pressure drop curves for every package as a function of the superficial air speed are presented in Figure A3. The pressure loss coefficient (ξ , $\text{Pa}\cdot\text{s}^2\cdot\text{m}^{-6}$) was computed using Eq. A1, assuming a quadratic dependency with the volumetric flow rate, and thus the superficial airspeed (U_{inlet} , $\text{m}\cdot\text{s}^{-1}$) (Defraeye et al., 2015).

$$\Delta P = \xi (A_{\text{channel}} U_{\text{inlet}})^2 \quad (\text{A1})$$

Here, A_{channel} is the cross-sectional area of channel [m^2]. For the flow-wrap packages, the pressure loss coefficient was computed by accounting for the free area ratio, as the package was not perfectly blocking the channel walls (Getahun et al., 2017). The free area ratio corresponds to the ratio of the open area to the total channel area in the flow direction.



FigureA3: Pressure drop across the package for horizontal airflow across a no bypass channel. For open punnet trays, the height of the channel was set to the height of a typical reusable packaging crate, i.e., 10.5 cm (IFCO, 2022). The pressure loss coefficient (ξ , $\text{Pa}\cdot\text{s}^2\cdot\text{m}^{-6}$) was computed by fitting a quadratic model in Microsoft Excel (2016). The R^2 values for the fitted curve were greater than 0.999 for all the curves and therefore not reported.

A.5 Additional packaging metrics

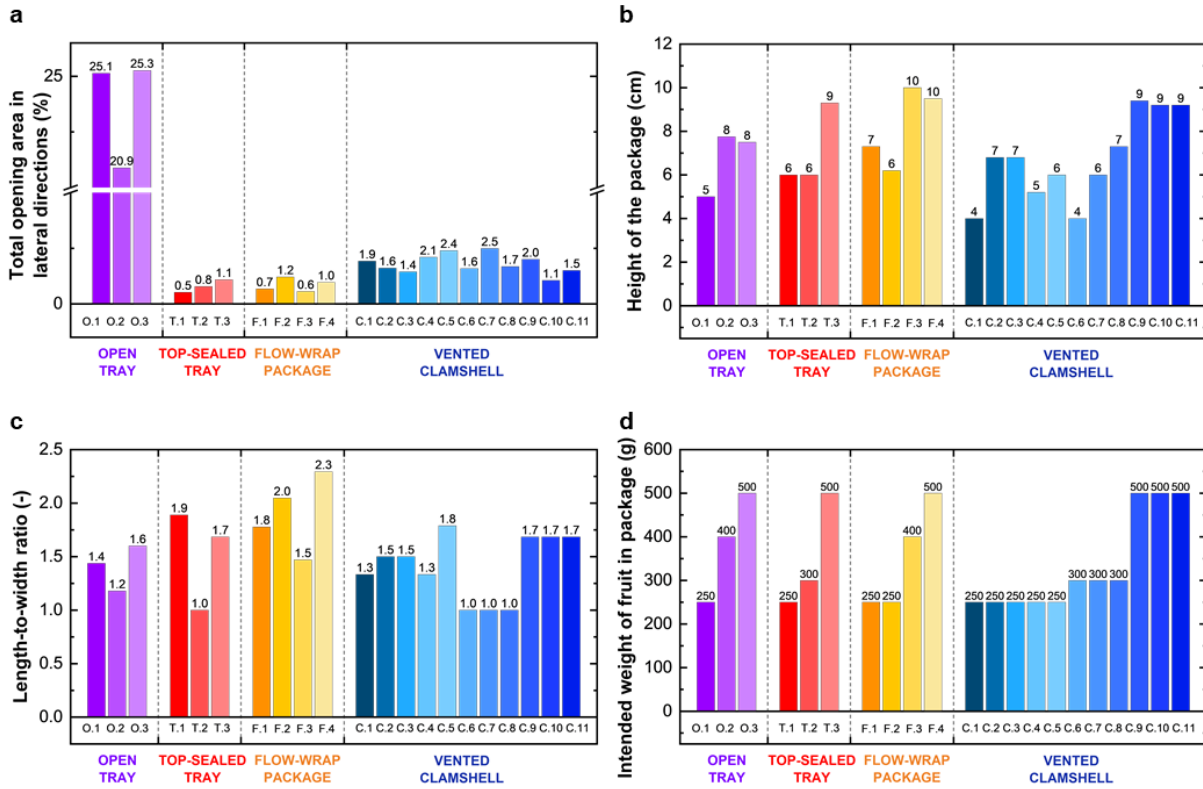


Figure A4: Additional packaging-related metrics for the 21 packages evaluated in this study: (a) Total open area in lateral directions (%); (b) Height of the package (cm); (c) Length-to-width ratio (-); (d) Intended weight of fruit in the package (g).

A.6 Grid sensitivity analysis and mesh elements

Our analysis shows that mesh convergence is more critical at higher air speeds, due to turbulent air flow. Therefore, for the grid sensitivity analysis, we target the convergence of the temperature of a fruit in the topmost layer of package during pre-cooling, after a time of 1 hour, which is close to the seven-eighths cooling time of the fruit. We investigate 5 meshes, with mesh elements ranging between 1.0×10^3 and 2.3×10^6 elements. As the underlying physics for all models is similar, we determine the optimal mesh settings for package C2 and use the same mesh settings for all other packages. The findings of our grid sensitivity analysis are presented in Figure A5 a. The corresponding number of elements for the 21 packages investigated in this study are indicated in Figure A5 b.

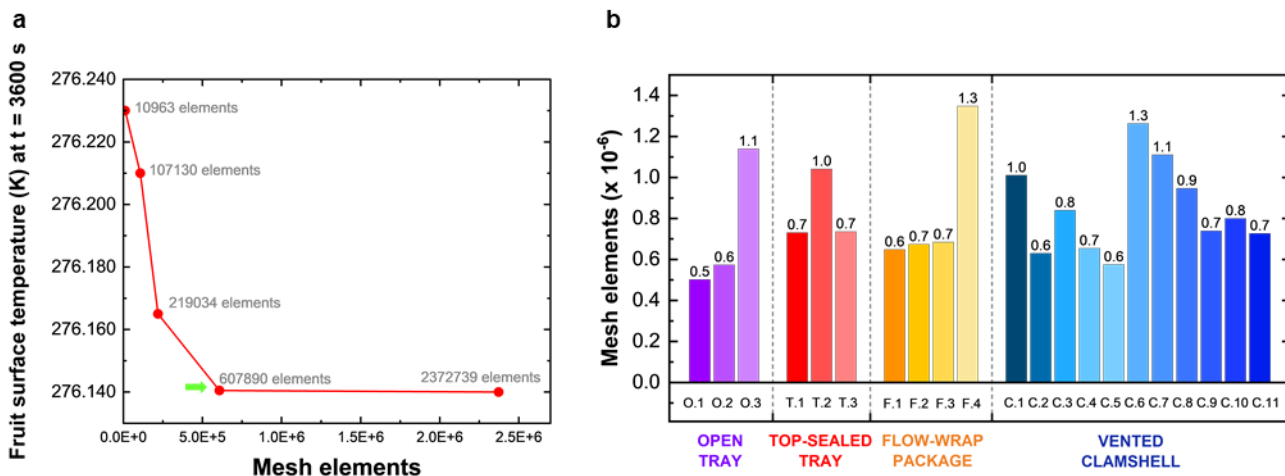


Figure A5: Grid sensitivity analysis: (a) Fruit surface temperature (K) during pre-cooling ($U_{upstream} = 1 \text{ m}\cdot\text{s}^{-1}$) for a fruit in the top layer of package C2. The green arrow indicates the mesh with optimal settings for the physics-based models that we implemented; (b) Number of mesh elements for the different packages based on the same mesh settings as the optimal mesh for package C2.

A.7 Model validation in a climate chamber

Figure A6 shows a comparison of the values predicted by the model and the values measured from climate chamber experiments. We observe a good agreement with measured and simulated values. For fruit temperature, we observe a slight lag. This is primarily because the simulated value corresponds to the volume-averaged fruit temperature, whereas the measured values correspond to point measurements inside the fruit. It is quite well-acknowledged that in a cold chain, $T_{\text{fruit,surface}} < T_{\text{fruit,average}} < T_{\text{fruit,core}}$. In this sense, the predicted and measured values show a good agreement. For relative humidity measurements, while one sensor shows a good agreement with the simulated value, the second sensor data shows some deviation (up to $\pm 10\%$). However, in the simulation, we predict the average relative humidity in the package headspace. On the other hand, the sensors only provide a point measurement of the relative humidity. This explains the observed differences. Altogether, the averaged value of simulated relative humidity across the entire supply chain was within 2% of the measured value, which is lower than the accuracy of the sensor.

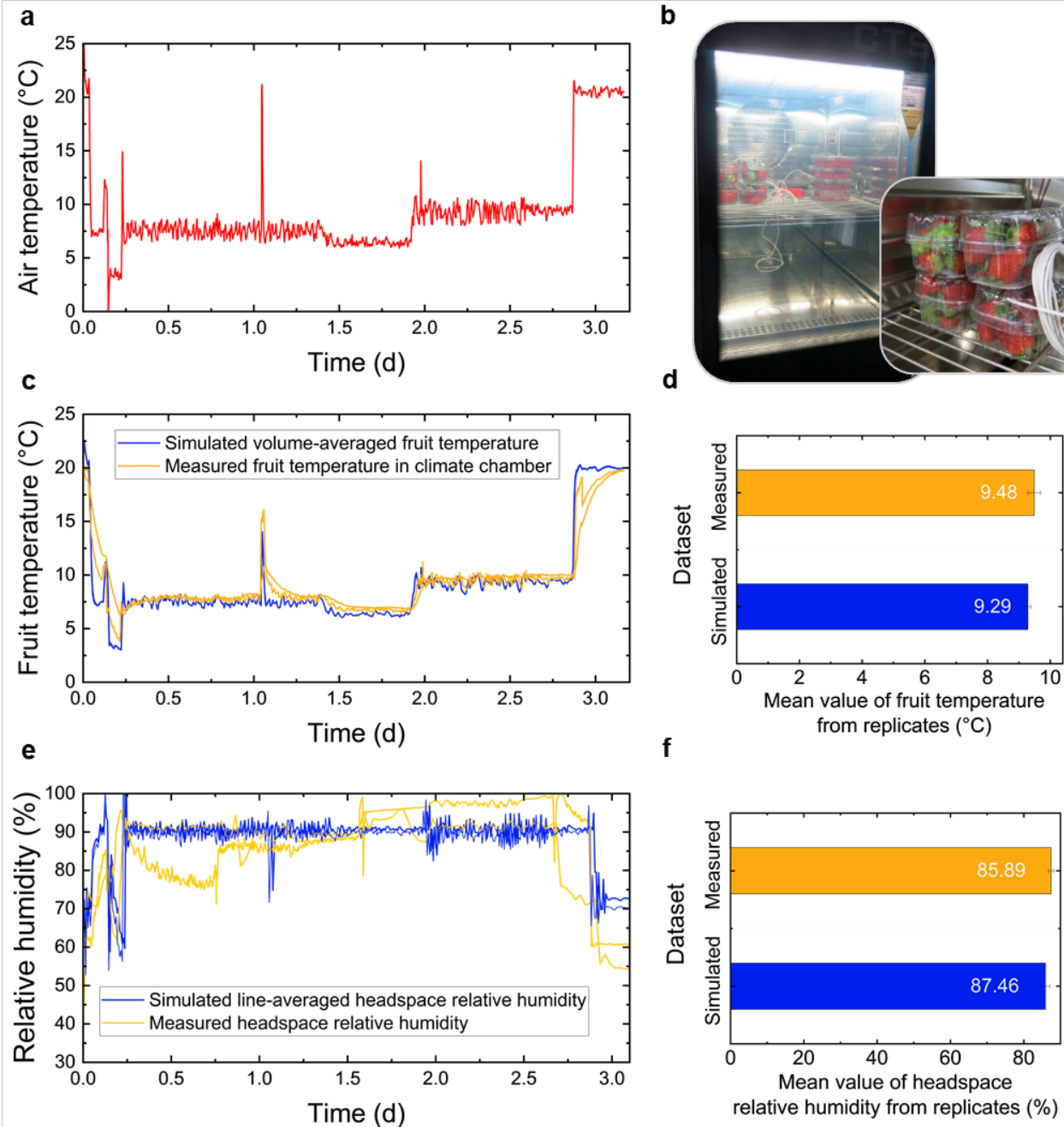


Figure A6 Validation of the heat and moisture transport models in a climate chamber: (a) Air temperature set for the chamber; (b) Photograph of the set-up; (c, d) Comparison between measured and simulated fruit temperature profile; (e, f) Comparison between measured and simulated headspace relative humidity inside the package.

A.8 Variability within the packages

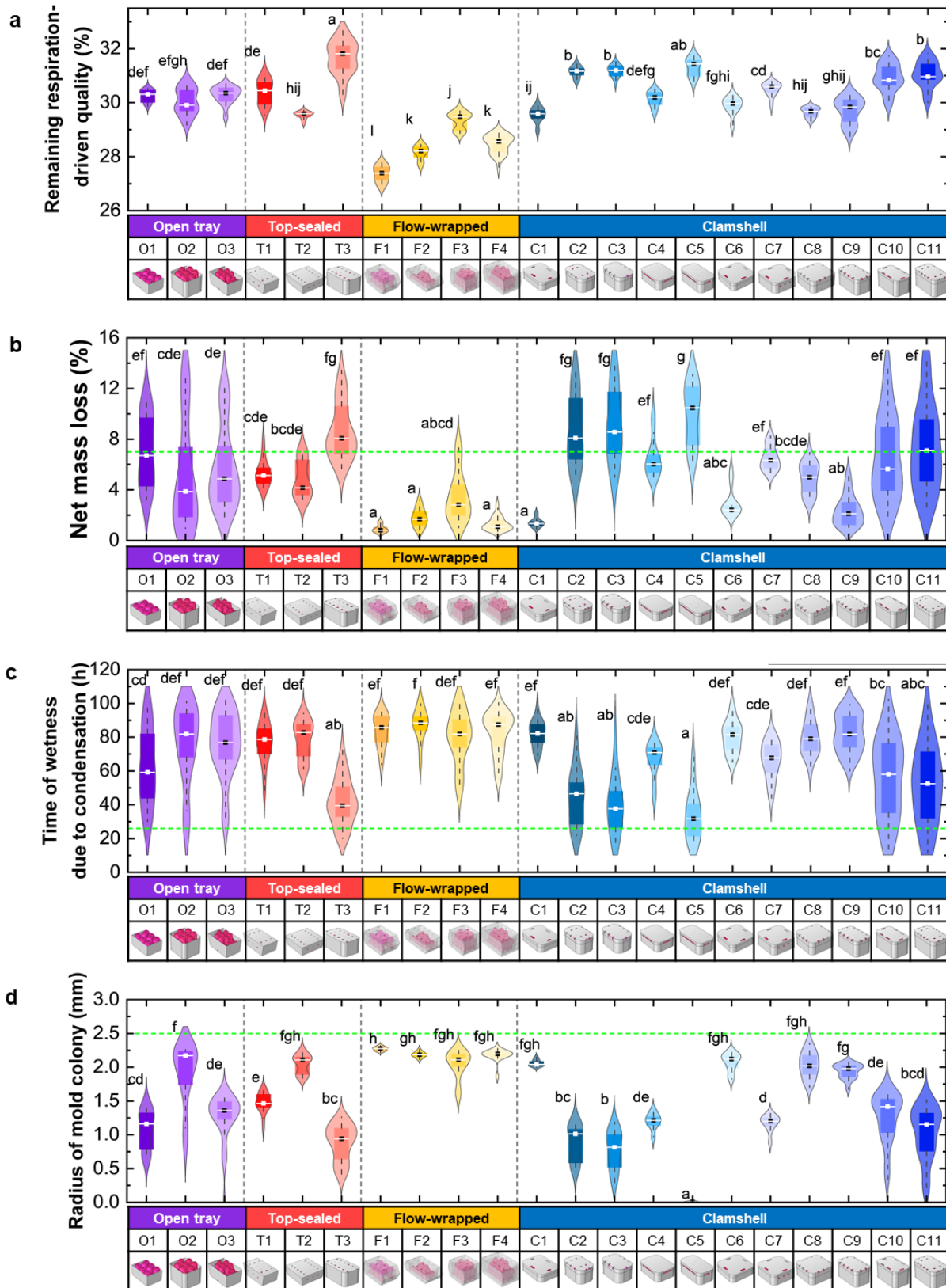


Figure A7: Violin plots showing the spread in the fruit quality metrics within the same package at the end of the simulated supply chain ($t = 4.5$ d). The violin plot encloses a box-and-whisker plot, where the box encloses fruit in the 25-75 percentile and the whiskers represent the range within $1.5 \times$ interquartile range. (a) Remaining respiration-driven fruit quality (%); (b) Net mass loss for fruit (%); (c) Time of wetness due to condensation (h); (d) Radius of *B. cinerea* colony (mm). The dotted green line indicates the threshold for acceptable values for each of the quality attributes.

References

- Defraeye, T., Cronjé, P., Berry, T., Opara, U.L., East, A., Hertog, M., Verboven, P., Nicolai, B., 2015. Towards integrated performance evaluation of future packaging for fresh produce in the cold chain. *Trends Food Sci Technol* 44, 201–225. <https://doi.org/10.1016/J.TIFS.2015.04.008>
- Getahun, S., Ambaw, A., Delele, M., Meyer, C.J., Opara, U.L., 2017. Analysis of airflow and heat transfer inside fruit packed refrigerated shipping container: Part II – Evaluation of apple packaging design and vertical flow resistance. *J Food Eng* 203, 83–94. <https://doi.org/10.1016/J.JFOODENG.2017.02.011>
- Han, J.W., Qian, J.P., Zhao, C.J., Yang, X.T., Fan, B.L., 2017. Mathematical modelling of cooling efficiency of ventilated packaging: Integral performance evaluation. *Int J Heat Mass Transf* 111, 386–397. <https://doi.org/10.1016/j.ijheatmasstransfer.2017.04.015>
- IFCO, 2022. Redefining the fresh grocery supply chain | IFCO [WWW Document]. URL <https://www.ifco.com/> (accessed 2.9.22).
- Li, C., Tang, H., Wang, J., Zhong, Z., Li, J., Wang, H., 2021. Field study to characterize customer flow and ventilation rates in retail buildings in Shenzhen, China. *Build Environ* 197, 107837. <https://doi.org/10.1016/J.BUILDENV.2021.107837>
- Opara, U.L., Zou, Q., 2007. Sensitivity analysis of a CFD modelling system for airflow and heat transfer of fresh food packaging: Inlet air flow velocity and inside-package configurations. *International Journal of Food Engineering* 3, 1–13. <https://doi.org/10.2202/1556-3758.1263>
- Silva, W.P. da, Carmo, J.E.F. do, Silva, C.M.D.P.S. e, Aragão, R.F., Silva, W.P. da, Carmo, J.E.F. do, Silva, C.M.D.P.S. e, Aragão, R.F., 2017. Determination of Convective Heat Transfer Coefficient During Cooling of an Individual Strawberry Fruit Using Different Methods. *International Review of Physics (IREPHY)* 11, 19–26. <https://doi.org/10.15866/IREPHY.V11I1.12144>
- Thompson, J.F., Mitchell, F.G., Rumsay, T.R., 2008. Commercial cooling of fruits, vegetables, and flowers. University of California, Agriculture and Natural Resources, p. 61.
- Wu, W., Cronjé, P., Verboven, P., Defraeye, T., 2019. Unveiling how ventilated packaging design and cold chain scenarios affect the cooling kinetics and fruit quality for each single citrus fruit in an entire pallet. *Food Packag Shelf Life* 21. <https://doi.org/10.1016/j.fpsl.2019.100369>